Revue Paralia, Volume 14 (2025) pp s03.13-s03.22
Keywords: Marine Energy and Resources, Hydrodynamics, Floating Offshore Wind Turbines (FOWT).

Numerical study of the response of floating wind turbines via computational fluid dynamics

Giacomo DIECI[1,2], Benjamin BOUSCASSE[1], Vincent LEROY[1], Sandrine AUBRUN[1], Marie-Laure DUCASSE[2]

1. Nantes Université, École Centrale Nantes, CNRS, LHEEA, UMR 6598, Nantes, France.
2. SAIPEM SA, Montigny-le-Bretonneux, France.
giacomo.dieci@saipem.com

Abstract:
Offshore wind turbines are rapidly increasing in size to capture stronger winds further offshore. However, as water depths increase, the designs of bottom fixed offshore wind turbines are no longer suitable, thus needing floating wind turbines design for depths greater than 50 m.
The significant dimensions of these sub-structures may lead to significant hydroelastic phenomena, which can also affect the elastic response of the tower, and so cannot be neglected. Reliable design of the floating substructures is necessary to avoid exciting certain eigen frequencies at low and high frequencies, with repercussions on the operation and fatigue life of the turbine. From a hydrodynamic point of view, a number of authors has carried out the study of seakeeping using high-fidelity CFD codes, then by characterising the fluid-dynamic constraints by solving the Navier Stokes equations using the finite volume method. An extension of these numerical models would also allow the flexibility of the structure to be taken into account.
The aim of the present work is to reproduce the experimental results obtained by (LEROY *et al.*, 2022) on a flexible SPAR platform model at the hydrodynamic and ocean engineering basin of Ecole Centrale de Nantes. The use of a high-fidelity numerical model (CFD) will be examined in order to study the floater dynamic response observed during the experimental campaign at the wave basin.

Paper selected during the colloquium "XVIIIèmes Journées Nationales Génie Côtier Génie Civil", Anglet (France), 25-27 June 2024.
Received 11 July 2024, accepted 26 January 2025, available online 10 February 2025.
Translated version not certified, published under the responsibility of the authors.

How to cite the original paper:
DIECI G., BOUSCASSE B., LEROY V., AUBRUN S., DUCASSE M.-L. (2025). *Étude de la réponse des éoliennes flottantes par des moyens de calculs haute-fidélité*. Revue Paralia, Vol. 14, pp s03.1–s03.12. DOI: https://doi.org/10.5150/revue-paralia.2025.s03

1. Introduction

The design objectives of floating offshore wind turbine platforms are mainly addressed to limit angular movements in order to increase productivity, to reduce horizontal movements in order to minimise loads on the mooring lines and to minimise structural stresses. The aim of this design process is to decrease the Levelized Cost of Energy, thus to reduce maintenance and investment costs while maximising performances.

One of the studied designs for floating wind turbines is the SPAR platform, which often consists of two cylindrical regions connected by a linearly reduced tapered region. Systems in the SPAR category achieve static stability in the pitch and roll degrees of freedom by lowering the centre of gravity with respect to the centre of buoyancy, so as to achieve a sufficiently high positive longitudinal and transverse metacentric height. (JONKMAN, 2010) provides an outstanding example of such a prototype.

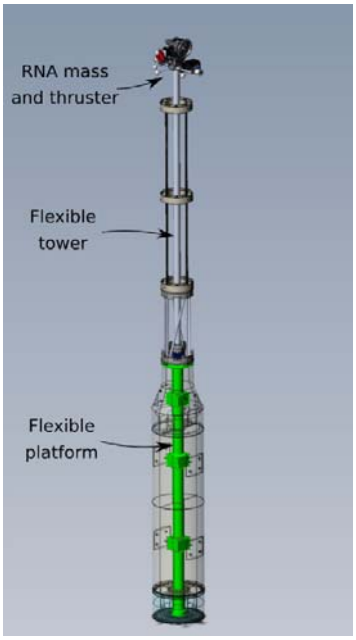

Figure 1. (LEROY et al., 2022) CAD view of the FOWT model.

The SPAR platform considered in this work was designed at Centrale Nantes, (ARNAL, 2020), to support the 10 MW DTU wind turbine. In this first design, the platform model was completely rigid. In the case examined in this work (LEROY *et al.*, 2022) the objective was to respect the Froude similarity at 1:40 scale with respect to the hydrodynamic response of the rigid body, as well as concerning the first mode of fore-aft bending mode frequency of a large FOWT with a nominal power of 10 MW, equal to 0.4 Hz at full scale. Figure 1 shows the CAD model of the floating platform at 1:40 scale. In order to scale correctly the eigen frequency of the first fore-aft bending mode of the whole system, the bending stiffness was reduced between the real scale and the model scale. To achieve this, an internal aluminium element (shown in green) of smaller diameter and

thinner thickness than the original floater geometry was used, around which elements were installed to reconstitute the complete floater geometry.
In this work, an attempt is made to obtain the response of the floating wind turbine model described above by means of high-fidelity codes (CFD), with regard to the solution of the fluid dynamics equations. The cases of decay tests and regular wave excitation are presented, comparing them with experimental values.

2. Numerical model

The CFD tool used in this work is named foamStar, which is developed jointly by École Centrale Nantes and Bureau Veritas, based on the OpenFOAM® version 5 open-source libraries.

2.1 foamStar : incompressible two-phase Navier-Stokes equations solver

In an Eulerian representation of the flow, an appropriate scheme must be introduced to recognise discontinuity surfaces such as the free surface. In foamStar, a phase indicator function α is used, such that $\alpha = 1$ for a water-filled mesh, and $\alpha = 0$ for meshes immersed in air. Other methods can be found in (FERZIGER *et al*., 2020). In this way, the density and dynamic viscosity are averaged by α:

$$\rho = \alpha\rho_{water} + (1-\alpha)\rho_{air} \quad (1)$$

$$\mu = \alpha\mu_{water} + (1-\alpha)\mu_{air} \quad (2)$$

It can be shown that, assuming the fluid is incompressible, substituting equation (1) into the continuity equation gives the volume fraction transport equation (HIRT & NICHOLS, 1981).
Therefore, given the above formulations for ρ and μ, the momentum equation of the Navier Stokes equations can be written as follows:

$$\frac{\partial(\rho\boldsymbol{u})}{\partial t} + \nabla\cdot(\rho\boldsymbol{u}\boldsymbol{u}) = -\nabla p_d - (\boldsymbol{g}\cdot\boldsymbol{x})\nabla\rho + \nabla\cdot(\mu\nabla\boldsymbol{u}) + \nabla\mu\cdot\nabla\boldsymbol{u}^T \quad (4)$$

where $\boldsymbol{u}$ denotes the velocity field, $\boldsymbol{g}$ the gravitational field, $\boldsymbol{x}$ the position vector with respect to the inertial reference frame and p_d the dynamic pressure. It should be noted that surface tension effects at the interface have been neglected. For more details, please refer to the PhD thesis of (KIM, 2021).
In the present work, the effect of turbulence on the mean fluid flow was modelled using the Eddy viscosity model proposed by (LARSEN & FUHRMAN, 2018), named $fs\ k-\omega\ SST$.

2.2 Coupling between stream function and CFD

The generation and propagation of waves towards the body are reproduced based on the stream function theory, which enables efficient and accurate and fully non-linear resolution of regular waves up to the breaking limit, assuming that the fluid is incompressible, that the flow is irrotational and that viscous effects are negligible. In order

to reproduce the wave conditions measured during the experimental tests, the CN-Stream code developed at École Centrale de Nantes by (DUCROZET *et al.*, 2019) was used, taking into account a Numerical Wave Tank (NWT) of the same size as the experimental tank. As shown in Figure 2, the coupling of the NWT domain with the pure CFD domain, represented by dashed lines in red, is achieved in this work through relaxation zones, whose range was 1.5λ or $1.5\lambda_P$ (denoting with λ_P the equivalent wave length for an irregular sea state, obtained by the dispersion relation with the peak period T_P). For more information on this coupling method, refer to the thesis of (LI, 2018). The discretised domain covers in x and y a distance of 4 λ, ranging from the actual basin depth of -5 m to 3.25 m, a height considered sufficient for mesh diffusion issues.

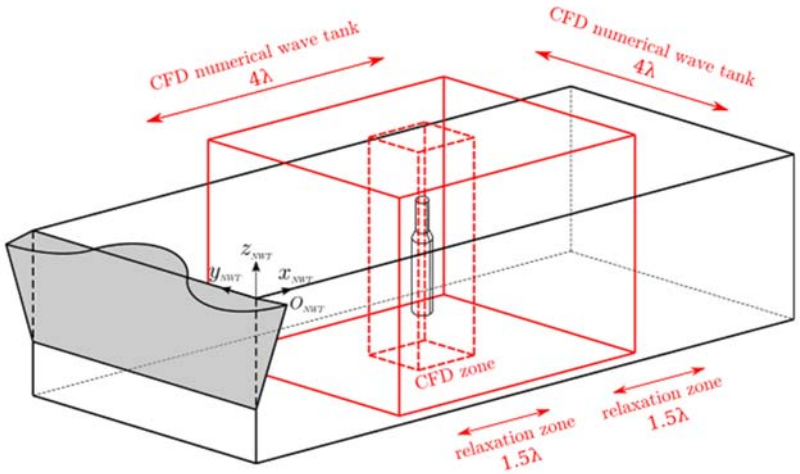

Figure 2. Representation of the numerical wave basin. The pure CFD zone is depicted in red, while the NWT zone in black.

2.3 Mooring lines dynamics : MoorDyn

Mooring lines forces were simulated via coupling of foamStar with MoorDyn® (HALL & GOUPEE, 2015), developed at the NREL in USA. The latter, based on lumped-mass theory, allows lines to be discretised into a finite number of segments of constant mass, volume, elastic properties and hydrodynamic coefficients. Further explanations can be found in (HALL & GOUPEE, 2015).

2.4 Rigid body dynamics

For the following mathematical formulation, reference is mainly made to (SHABANA, 2005) and (PEREZ, 2005). Hence, following the Euler's angles $\boldsymbol{\Theta}_{0b}$ notation introduced in (PEREZ, 2005) between the inertial reference frame $\mathcal{R}_0$ and the body fixed frame $\mathcal{R}_b$, the rigid body motion equations can be written as:

$$\boldsymbol{M}^b_{/O_g}\ddot{\boldsymbol{q}} = -\boldsymbol{Q}^b_{/O_g}\dot{\boldsymbol{q}} + \tau^b \quad (6)$$

where: $\boldsymbol{Q}^b_{/O_g}$ is the Coriolis-Centripetal matrix, $\boldsymbol{M}^b_{/O_g}$ is the generalized mass matrix with respect to the principal axis of inertia and $\boldsymbol{q} = [\boldsymbol{r}^0_{O_g/0}\ \boldsymbol{\Theta}_{0b}]$ are the generalized coordinates, being $\boldsymbol{r}^0_{O_g/0}$ the position vector of point O_g with respect to $\mathcal{R}_0$ and expressed in $\mathcal{R}_0$. Constraints forces were included in (6) following the stabilization method introduced by (BAUMGARTE, 1972), so as to prevent sway, roll and yaw motions. This results in the following system of ordinary differential equations to be solved:

$$\begin{cases} \boldsymbol{M}^b_{/O_g}\ddot{\boldsymbol{q}} = -\boldsymbol{Q}^b_{/O_g}\dot{\boldsymbol{q}} + \tau^b - \lambda \boldsymbol{C}_{\boldsymbol{q}}^T\ddot{\boldsymbol{q}} \\ \boldsymbol{C}_{\boldsymbol{q}}\ddot{\boldsymbol{q}} = -\dot{\boldsymbol{C}}_{\boldsymbol{q}}\dot{\boldsymbol{q}} - 2\alpha\dot{C}(\boldsymbol{q}) - \beta^2 C(\boldsymbol{q}) \end{cases} \quad (7)$$

where: $C(\boldsymbol{q})$ is the set of independent constraint equations, $\boldsymbol{C}_{\boldsymbol{q}}$ its Jacobian matrix, λ the vector of Lagrange's multipliers and α and β are parameters derived from the Baumgarte's stabilisation criterion.

3. Experimental end numerical set-up

Table 1 shows the geometry and mass properties of the built numerical model, representing the platform, tower and wind turbine assembly. For more information on these data, as well as on the layout and properties of the mooring lines, refer to (LEROY *et al.*, 2022). The height of the model with respect to the waterline has been defined so that hydrodynamic loads can be taken into account continuously in the event of a high wave or large motion (no change in the diameter of the waterline surface), thus avoiding non-physical water phenomena on deck.

Hereafter, the input data and results are presented at full scale, while all the simulations were carried out at 1:40 scale, thus respecting Froude similitude with wave basin tests. Body motions and rotations are expressed at the centre of gravity of the whole system (platform and wind turbine).

The numerical results were compared qualitatively with the following experimental tests:

a) Heave decay test, for an initial displacement of 2 m.
b) Pitch decay test, for an initial inclination of 5°.
c) Regular wave case, H=12 m, T=11.32 s and steepness of 6 %.

It should also be noted that for the decay tests, a calm water condition was imposed in the relaxation zones in order to avoid the reflection of radiation waves. In this case, a variable time step was used, setting the maximum Courant's number at 0.6.

In the case of wave-structure interaction, the elevation of the wave in the absence of the body was verified a priori, by comparing the results with measurements from the WG4 wave probe placed at the initial position of the platform. See (LEROY *et al.*, 2022) for more details. In order to considerably reduce the computational time, due to the symmetry of the problem, the domain was discretised only for $y > 0$, thus constraining the yaw, roll and yaw degrees of freedom. In the case of regular waves, a constant time step based on the wave period was used, thus equal to T/600.

Table 1. Global mass properties and geometry of the model (full scale)

Draft	*90*	*m*
Diameter below taper	*18*	*m*
Diameter at waterline	*11.2*	*m*
z of the top of the taper	*-5.48*	*m*
Length of the taper	*8*	*m*
Height of the model above the waterline	*32*	*m*
z of the COG with respect to the waterline	*-56.46*	*m*
Mass	*2.1343E+07*	*kg*
Iyy with respect to the COG	*5.0649E+10*	*kg.m^2*

4. Results

Equilibrium tests for each mesh used confirmed the mass properties and the discretization of the volume of water displaced for a given water draft. In fact, the displacements in the various degrees of freedom at equilibrium were negligible with respect to initial conditions.

Figures 3 and 4 show the results of the heave and pitch decay tests respectively. Figure 5 shows the calibration of the free surface elevation at target body position. The time at which the waves reach the body after being reflected at the end of the basin has been highlighted in the figures and has been estimated using the group velocity calculated by the linear Airy's solution. The corresponding pitch, surge and heave motions are shown in Figures 6, while Figure 7 shows the Fourier's transform of the pitch motion.

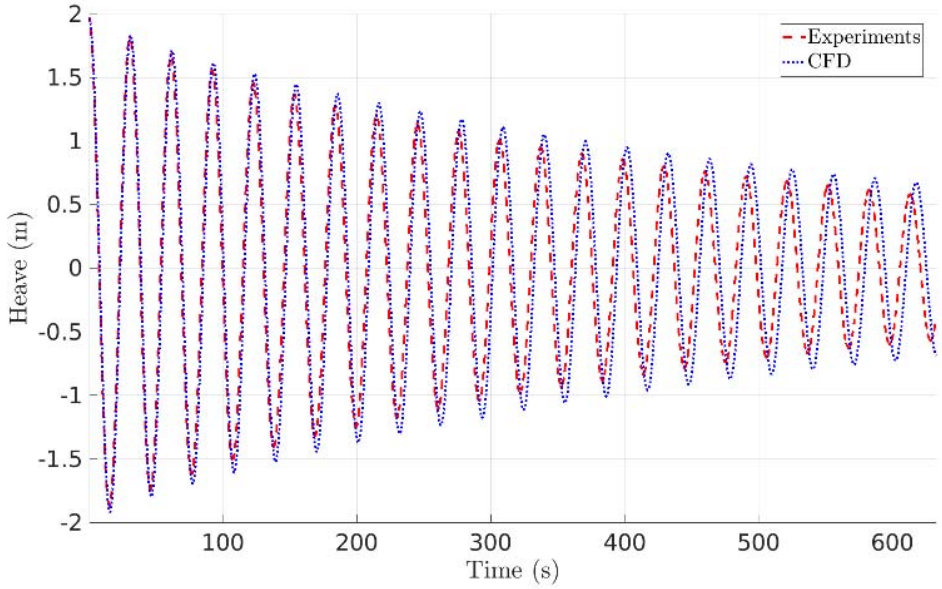

Figure 3. Heave decay test.

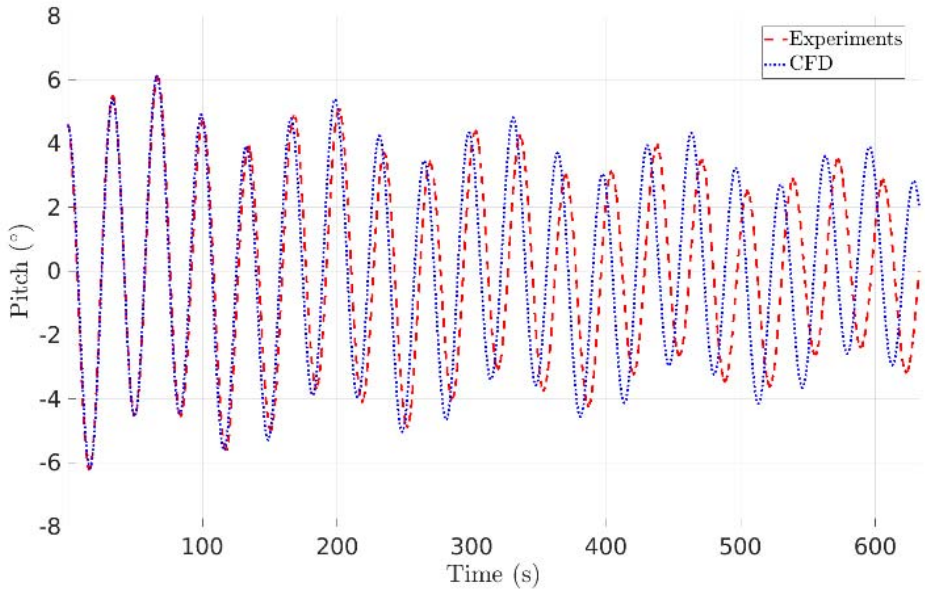

Figure 4. Pitch decay test.

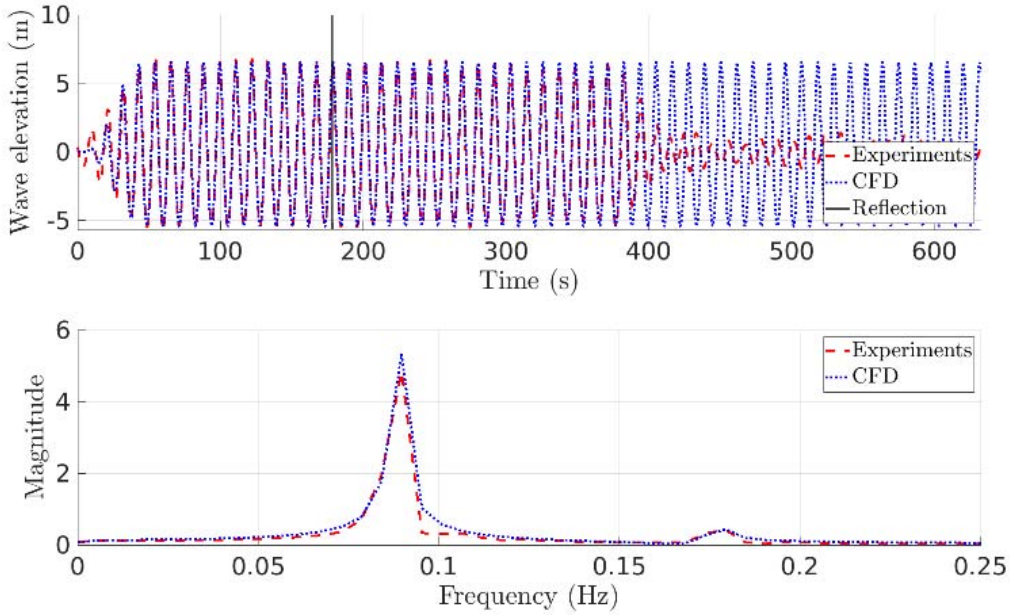

Figure 5. Calibration of wave elevation to body position and the absence of the latter, H=12 m, T=11.32 s.

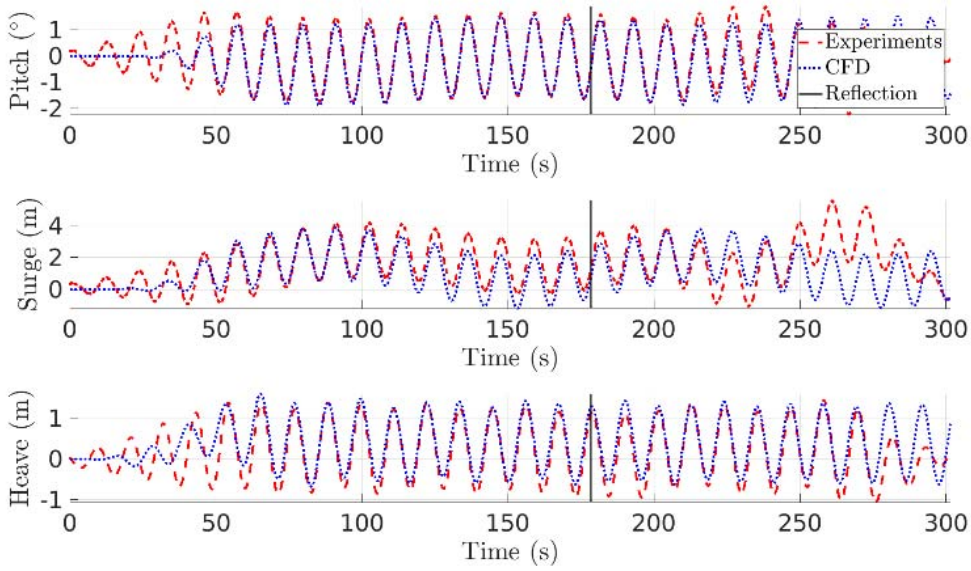

Figure 6. Time series of pitch, surge and heave motions. H=12 m, T=11.32 s.

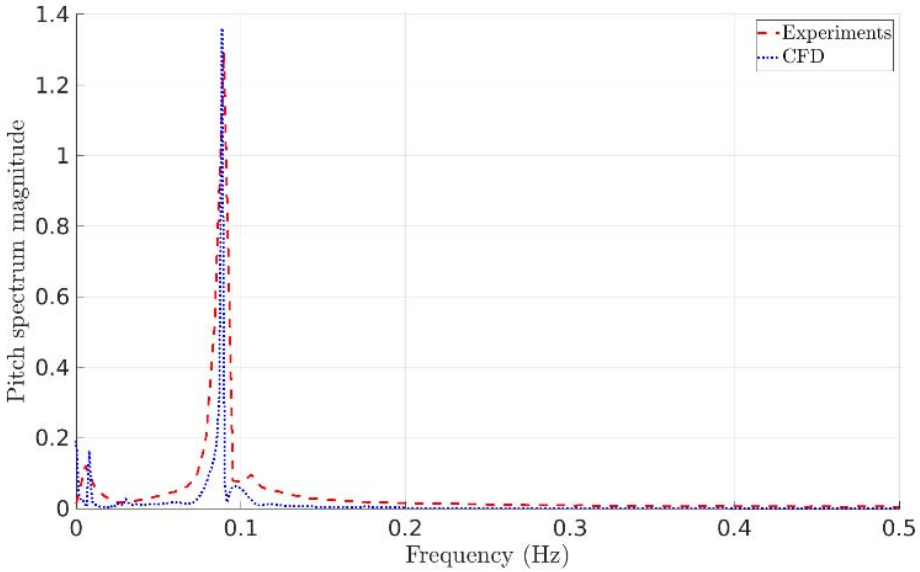

Figure 7. Pitch motion response spectrum. H=12 m, T=11.32 s.

5. Discussions

The decay tests presented in Figures 3 and 4 confirmed the validity of the model carried out in the absence of waves, thus fair computations of restoring, added mass and damping terms. The increase in the differences between the experimental and numerical values was attributed to the truncation of the domain, which introduces an error especially in the evaluation of linear hydrodynamic damping, i.e. in the generation of waves by the body

in the far field through its motion, mechanism by which it transfers energy to the surrounding fluid-dynamic field. In fact, there is an increasing phase difference which may be linked to this uncertainty in hydrodynamic damping. A more detailed study should be carried out to understand the importance of the accumulated numerical errors on these results. However, the agreement between the curves at the start of the simulation suggests that the release of vortices during large-amplitude oscillations is well reproduced, and thus the quadratic damping terms.

Figure 5 shows excellent agreement between experimental values and numerical results, confirming both the good performances of the code in the case of wave propagation and the coupling between the CN-Stream code and foamStar. The validity of the coupling between foamStar and CN-Stream is further confirmed by the Fourier's transform of the wave elevation signal, which shows that the non-linearity of the incident wave field is also well represented numerically in the frequency domain, where there is agreement even at higher harmonics, $f > 1/T$.

From a qualitative point of view, with reference to Figure 6, the response of the platform also shows agreement between the numerical and experimental steady-state results. The different transient responses are due to the different initial ramps of the incident waves and to the management of the transient state within the code. In fact, the use of the stream function assumes a stationary solution of the wave field, which therefore cannot take into account the correct spatial propagation of the wave front from the wave generator to the position of the body. However, analysis of the frequency of the pitch motion shows good agreement between the results, even at low frequencies.

6. Conclusion

The dynamic response of the floating platform observed in the basin, even in the presence of regular waves, was faithfully reproduced by foamStar. However, the decay test curves in the pitch and heave degrees of freedom show increasing differences with the experimental values as the simulation time progresses, which was mainly attributed to the truncation of the simulated dynamic fluid field. On the other hand, the case of regular waves presented shows that the model manages to reproduce wave-body interactions even for waves that deviate significantly from linear theory, thus overcoming the limitations of methods based on the potential flow hypothesis.

Future developments in this work include the study of several wave cases, even irregular ones, and the inclusion of structural flexibility in the numerical model.

7. References

ARNAL V. (2020). *Experimental modelling of a floating wind turbine using a "software-in-the-loop" approach*. Thèse de Doctorat, École Centrale de Nantes.

BAUMGARTE J. (1972). *Stabilization of constraints and integrals of motion in dynamical systems*. Computer Methods in Applied Mechanics and Engineering, Vol. 1, No. 1, Elsevier BV, pp. 1-16. https://doi.org/10.1016/0045-7825(72)90018-7

DUCROZET G., BOUSCASSE B., GOUIN M., FERRANT P., BONNEFOY F. (2019). *CN-stream: Open-source library for nonlinear regular waves using stream function theory.* Ecole Centrale de Nantes.

FERZIGER J.H., PERIC M., STREET R.L. (2020). *Computational methods for fluid dynamics.* Springer International Publishing, 596 p. https://doi.org/10.1007/978-3-319-99693-6

HALL M., GOUPEE A. (2015). *Validation of a lumped mass mooring line model with DeepCwind semisubmersible model test data*. Ocean Engineering, Volume 104, 590-603. https://doi.org/10.1016/j.oceaneng.2015.05.035

HIRT C. W., NICHOLS B.D. (1981). *Volume of fluid (VOF) method for the dynamics of free boundaries. Journal of Computational Physics.* Vol. 39, No. 1, 201-225. https://doi.org/10.1016/0021-9991(81)90145-5

JONKMAN J. (2010). *Definition of the floating system for phase IV of OC3.* Rapport Technique, NREL.

KIM Y.J. (2021). *Numerical improvement and validation of a naval hydrodynamics CFD solver in view of performing fast and accurate simulation of complex ship-wave interaction*. Thèse de doctorat, Ecole Centrale de Nantes, (NNT : 2021ECDN0031). ⟨tel-03530266⟩

LARSEN B.E., FUHRMAN D.R. (2018). *On the over-production of turbulence beneath surface waves in Reynolds-averaged Navier-Stokes models.* Journal of Fluid Mechanics, Vol. 853, Cambridge University Press (CUP). https://doi.org/10.1017/jfm.2018.577

LEROY V., DELACROIX S., MERRIEN A., BACHYNSKI E., GILLOTEAUX J.-C. (2022). *Experimental investigation of the hydro-elastic response of a spar-type floating offshore wind turbine*. Ocean Engineering, Vol. 255, 111430. https://doi.org/10.1016/j.oceaneng.2022.111430

LI Z. (2018). *Two-phase spectral wave explicit Navier-Stokes equations method for wave structure interactions.* Thèse de doctorat, Ecole Centrale de Nantes.

PEREZ T. (2005). *Ship motion control*. Springer, 300 p. https://doi.org/10.1007/1-84628-157-1

SHABANA A.A. (2005). *Dynamics of multibody systems,* Third Edition. Cambridge University Press, 374 p. https://doi.org/10.1017/CBO9780511610523